Optimal design of resonant piezoelectric buzzer from a perspective of vibration-absorber theory

Mingsian R. Bai,[a] Rong-Liang Chen, and Chung-Yuan Chuang
Department of Mechanical Engineering, National Chiao-Tung University, 1001 Ta-Hsueh Road, Hsin-Chu 300, Taiwan

Cheng-Sheng Yu and Huey-Lin Hsieh
Ceramic Materials Section, New Materials Research & Development Department, China Steel Corporation, 1 Chung Kang Road, Hsiao Kang, Kaohsiung 812, Taiwan

(Received 24 November 2006; revised 13 June 2007; accepted 14 June 2007)

In this paper, an optimization technique is presented for the design of piezoelectric buzzers. This design technique aims at finding the optimal configuration of the coupled cavity and diaphragm structure to maximize the sound pressure output. Instead of measuring the material constants of the piezoelectric ceramic and the metal diaphragm, an "added-mass method" is developed to estimate the equivalent electromechanical parameters of the system on which an analogous circuit can be established. The electrical impedance and on-axis sound pressure level of the piezoelectric buzzer can be simulated by solving the loop equations of the electromechanoacoustical analogous circuit. An interesting finding of this research is that the nature of the piezoelectric buzzer bears remarkable resemblance to that in the dynamic vibration absorber theory. Much physical insight can be gained by exploiting this resemblance in search of the optimal configuration. According to the system characteristic equation, a design chart was devised to "lock" the critical frequency at which the system delivers the maximal output. On the basis of the analogous circuit and the vibration absorber theory, an optimal design was found with constrained optimization formalism. Experiments were conducted to justify the optimal design. The results showed that the performance was significantly improved using the optimal design over the original design. Design guidelines for the piezoelectric buzzers are summarized. © *2007 Acoustical Society of America.* [DOI: 10.1121/1.2756757]

PACS number(s): 43.38.Fx, 43.38.Ar, 43.40.Tm [AJZ] Pages: 1568–1580

I. INTRODUCTION

Piezoelectric buzzers are commonly used in many applications, such as household appliances, car security systems, medical apparatus, etc. They are essentially narrow-band devices intended to operate at the resonant frequency for large sound pressure output. In other words, the driving frequency generally coincides with the resonant frequency of the system to achieve the maximal efficiency. Although the buzzer technology is not new, this paper attempts to examine the devices in light of rigorous electroacoustic analysis. It is found from this research that interesting physical insights can be gained from these quite common devices. Useful guidelines for reaching optimal designs can also be derived from these findings.

A typical piezoelectric buzzer consisting of a piezoelectric diaphragm, a cavity with a port, and electrode terminals is shown in Figs. 1(a)–1(c). The piezoelectric diaphragm is generally made up of a piezoelectric ceramic disc attached to a slightly larger metal plate. Some studies on piezoelectric plates have been reported in the past. Caliano *et al.*[1] proposed a piezoelectric bimorph membrane sensor for pressure measurement. Tseng and Liou,[2] Dobrucki and Pruchnickli,[3] and Wang *et al.*[4] conducted theoretical and numerical investigations on the dynamic responses of bimorph piezoacoustic transducers. The dynamic behavior of a circular piezoelectric transducer was solved by numerical methods and compared to the results of the finite element method. Aronov[5,6] applied energy methods to analyze the piezoelectric transducers and established a model for simulation. A similar methodology was also applied to other piezoelectric transducers, e.g., panel speakers,[7] ultrasonic transducers,[8,9] etc. Caronti *et al.*[9] modeled a capacitive micromachined ultrasonic transducer by a two-port network. Gallas *et al.*[10] used lumped-element models to examine the frequency responses of a piezoelectric-driven synthetic jet actuator.

This paper aims at an in-depth analysis of the piezoelectric buzzer, with the emphasis on the interactions between the structural dynamics of the piezoelectric diaphragm and the acoustical response of the cavity and port. As will be demonstrated later in the paper, the physics underlying the coupled mechanical and acoustical system is surprisingly parallel to that of a *dynamic vibration absorber*.[11,12] It is this subtle mechanism that dictates the ultimate performance of the buzzer. By taking advantage of this mechanism, maximum sound pressure output can be attained. In addition, systematic search procedures can be employed to find optimal designs of the piezoelectric buzzer without time-consuming trial and error. To facilitate the design optimization, a simulation platform is established in the paper by using an experimental parameter identification method, the *added-mass*

[a]Author to whom correspondence should be addressed; electronic mail: msbai@mail.nctu.edu.tw

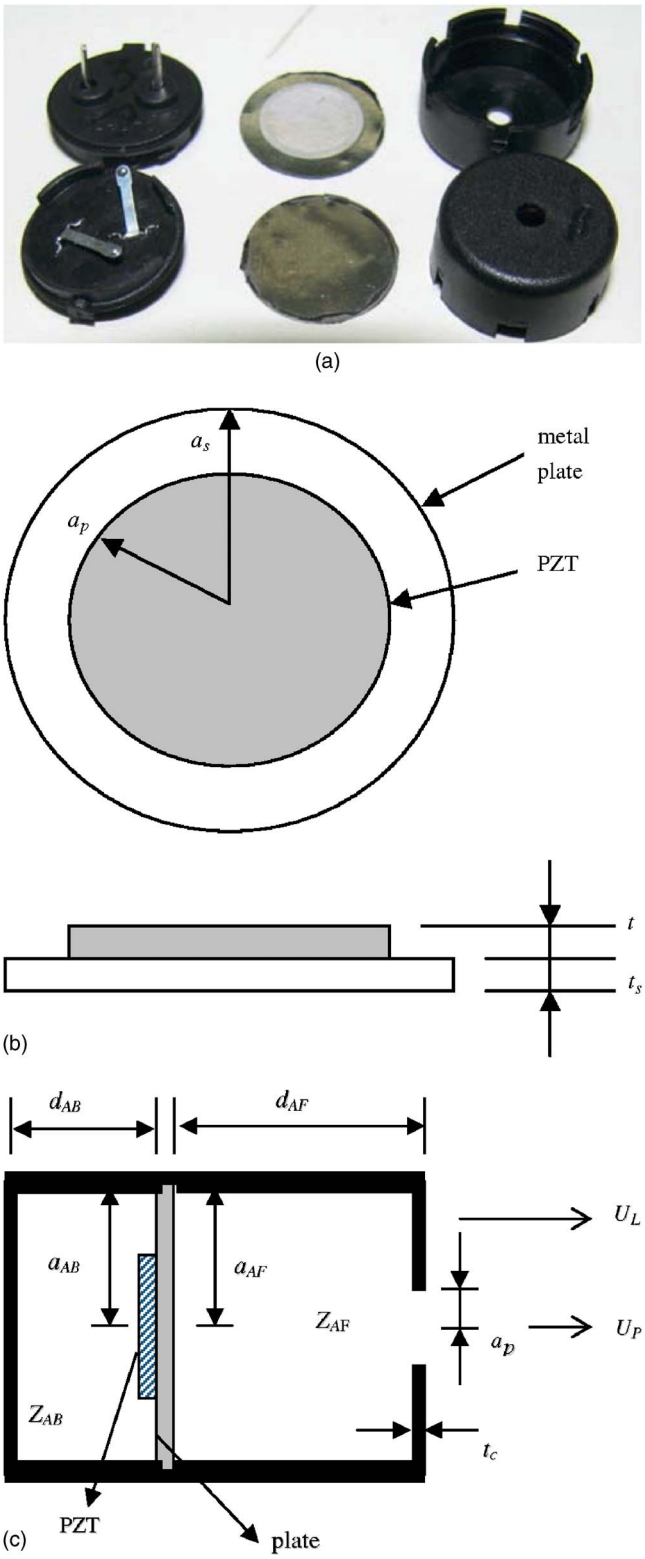

FIG. 1. (Color online) Piezoelectric buzzer, (a) Photo of the buzzer, (b) diaphragm structure, and (c) cross section of the piezoelectric buzzer.

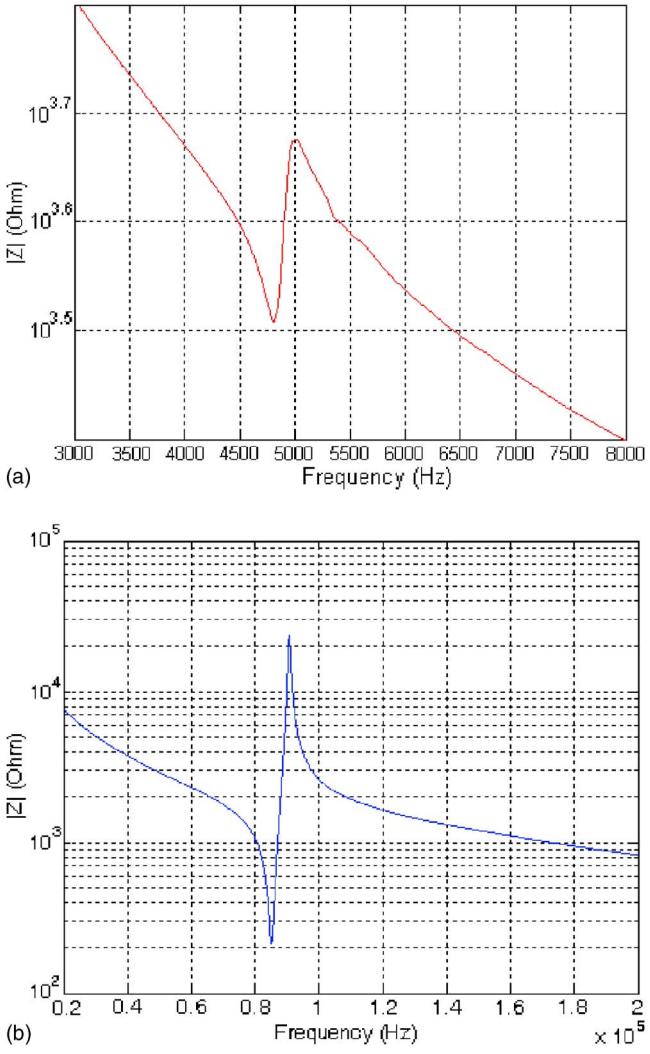

FIG. 2. (Color online) The measured electrical impedance of piezoelectric samples. (a) Rectangular plate of a standard PZT 5A and (b) piezoelectric diaphragm consisting of the PZT plate and the metal plate.

method, similar to that used for electrodynamic loudspeakers.[13,14] With the identified parameters, the electrical impedance and the on-axis pressure response of the piezoelectric buzzer can be calculated by solving the loop equations[15] of the electromechanmacoustical (EMA) analogous circuit.[13,14] On the basis of the dynamic vibration absorber theory, a characteristic equation can be derived for predicting the resonance frequencies of the coupled mechanical and acoustical system of the piezoelectric buzzer. A design chart method was thus developed according to the characteristic equation to determine the optimal cavity and duct dimensions. The method can also be extended to a broader context in which both mechanical and acoustical parameters need to be optimized. A constrained optimization technique is developed using sequential quadratic programming (SQP)[16–18] to optimize the design parameters. On-axis pressure is selected to be the objective function for optimization, whereas the driving frequency, elctroacoustical parameters, dimensions of the cavity and port, etc., are appropriately constrained. It will be demonstrated by simulations and experiments that the optimized design significantly improves the performance of the buzzer over the original design. The physical insights as well as guidelines found in the design optimization are summarized in Sec. V.

II. MODELING OF THE PIEZOELECTRIC BUZZER

A sample of a piezoelectric buzzer with a 12.7 mm diameter and 6 mm thickness is shown in Fig. 1(a). The piezo-

TABLE I. Dimensions of cavity of the piezoelectric buzzer.

Parameters	Dimension (mm)
Radius of rear cavity (a_{AB})	5.0
Height of rear cavity (d_{AB})	1.48
Radius of front cavity (a_{AF})	5.25
Height of front cavity (d_{AF})	3.08
Thickness of cavity (t_c)	0.76
Radius of port (a_p)	1.065
Radius of plate (a_s)	5.57
Thickness of plate (t_s)	0.05
Radius of PZT (a_p)	4.0
Thickness of PZT (t_p)	0.09

electric diaphragm is fitted in a plastic case. A pair of metal terminals are electrically connected to the piezoelectric diaphragm and drawn out from the back cover of the plastic case. The front portion of the buzzer consists mainly of a cavity with a circular port that serves as the sound outlet. The cross section of the piezoelectric buzzer is shown in Fig. 1(b) with dimensions indicated in Table I Figure 1(c) shows the diaphragm consisting of a circular piezoelectric ceramic (lead zirconate titanate, PZT 5A) and a circular plate (Fe-Ni alloy, Fe-60%, Ni-40%). By comparing the electrical impedance of this piezoelectric diaphragm [Fig. 2(a)] and that of a rectangular plate of standard PZT 5A sample without the metal plate [Fig. 2(b)], we found that the piezoelectric diaphragm exhibits basically similar characteristics to that of a piezoelectric ceramic alone. This suggests that the piezoelectric diaphragm can be modeled, in the low frequencies, by the same structure of the electromechanical analogous circuit in Figs. 3(a) and 3(b) as those used for a pure PZT sample. In order to determine the lumped electromechanical parameters in the circuit, a special experimental procedure was developed in this study and is detailed next.

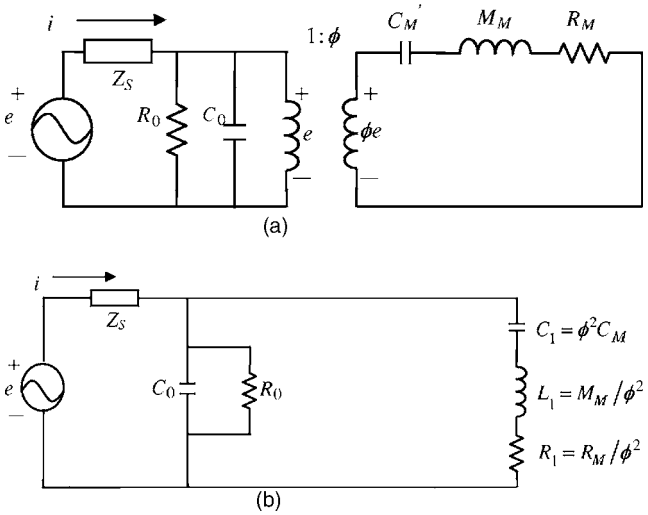

FIG. 3. Analogous circuit of the piezoelectric diaphragm. (a) The electrical and the mechanical circuits and (b) the circuit expressed in the electrical domain.

A. Parameter identification

Instead of calculating the lumped parameters using piezoelectric and other material constants, we opt to identify these parameters directly from electrical impedance measurement.[13] This approach, the *added-mass method*, was inspired by a commonly used method in identifying electrodynamic loudspeaker constants. Before the impedance measurement, the front cover of the buzzer must be removed, as shown in Fig. 4(a). Next, a 0.05 g clay patch is attached to

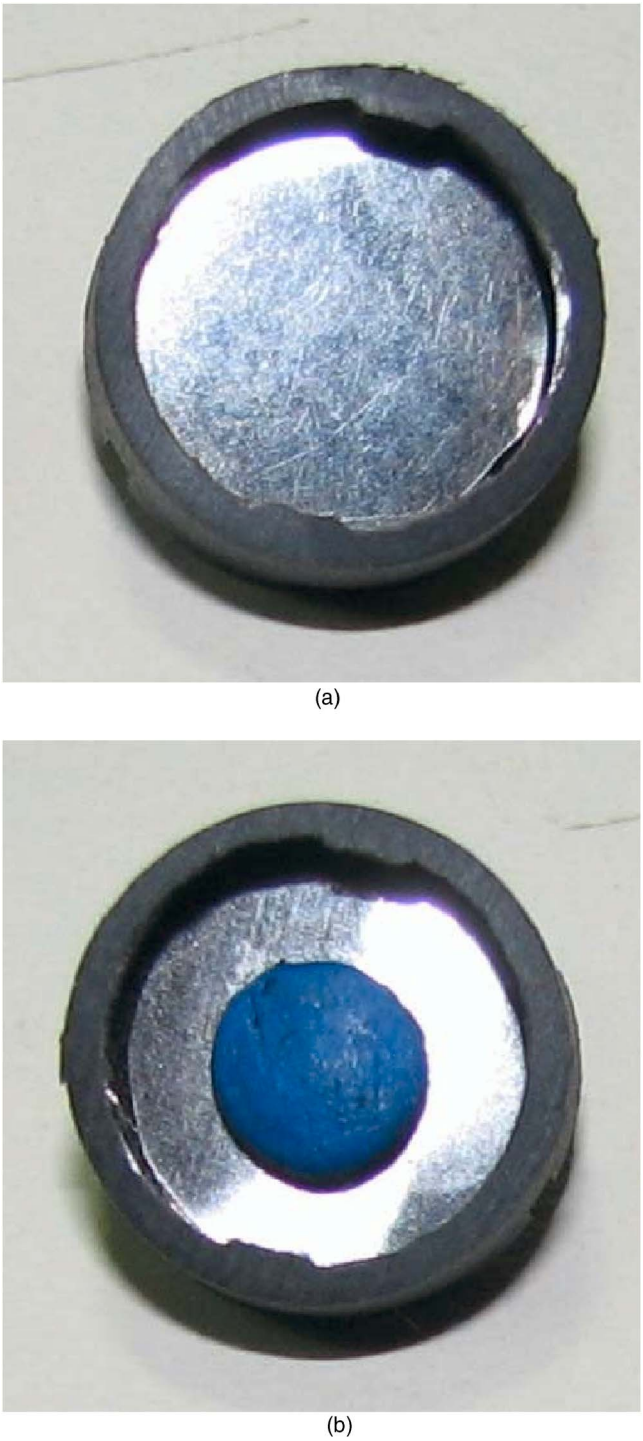

FIG. 4. (Color online) Piezoelectric buzzer without the front cover. (a) Photo of the buzzer, and (b) photo of the buzzer with the added mass on the diaphragm.

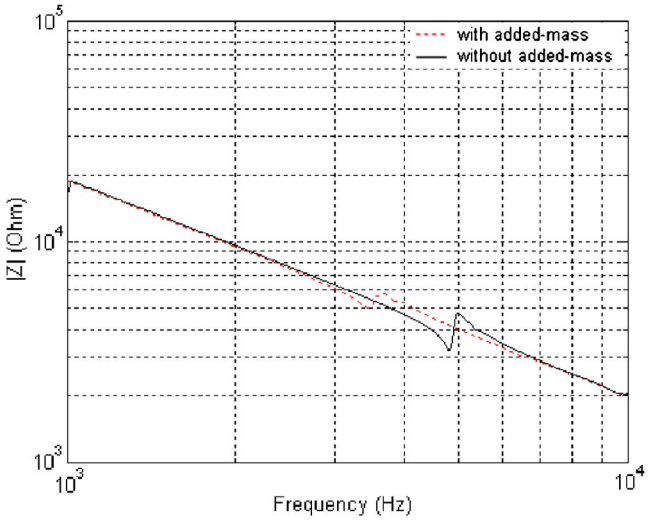

FIG. 5. (Color online) The measured electrical impedance of the buzzer, with and without the added mass.

the diaphragm, as shown in Fig. 4(b). The measured electrical impedance curves of the piezoelectric diaphragm with (solid line) and without (dashed line) the added mass are shown in Fig. 5. Clearly seen in the impedance curves, the resonant frequency (the trough in the curve) of the diaphragm has been decreased from 4875.0 to 3443.8 Hz because of the added mass.

The parameter identification procedure serves two purposes. First, the response of the buzzer, including electrical impedance, volume velocity, and sound pressure level (SPL), can be simulated and performance can be assessed on the basis of the EMA analogous circuit. Second, design optimization can be carried out on the platform of the identified model to determine the optimal loudspeaker parameters. The parameter identification procedure is outlined as follows.

1. Parameter estimation in the electrical domain

Figures 6(a) and 6(b) show a generic Nyquist plot of the electrical impedance and admittance of piezoelectric diaphragm (PZT + metal plate), respectively, from which the serial resonant frequency (f_s) and parallel resonant frequency (f_p) can be determined by locating the maxima of the real parts of the admittance ($G_{\max}$) and the impedance ($R_{\max}$), respectively. The Nyquist plot enables us to determine the parameters in Fig. 3(b). The dielectric losses (R_0) can be calculated from the minimum of the real part of admittance ($G_{\min}$),

$$R_0 = \frac{1}{G_{\min}}. \tag{1}$$

From the serial resonant frequency (f_s) and parallel resonant frequency (f_p); we may calculate the static capacitance (C_0), dynamic capacitance (C_1), inductance (L_1), and quality factor (Q) as follows:[19]

$$C_0 = (f_s/f_p)^2 C_f, \tag{2}$$

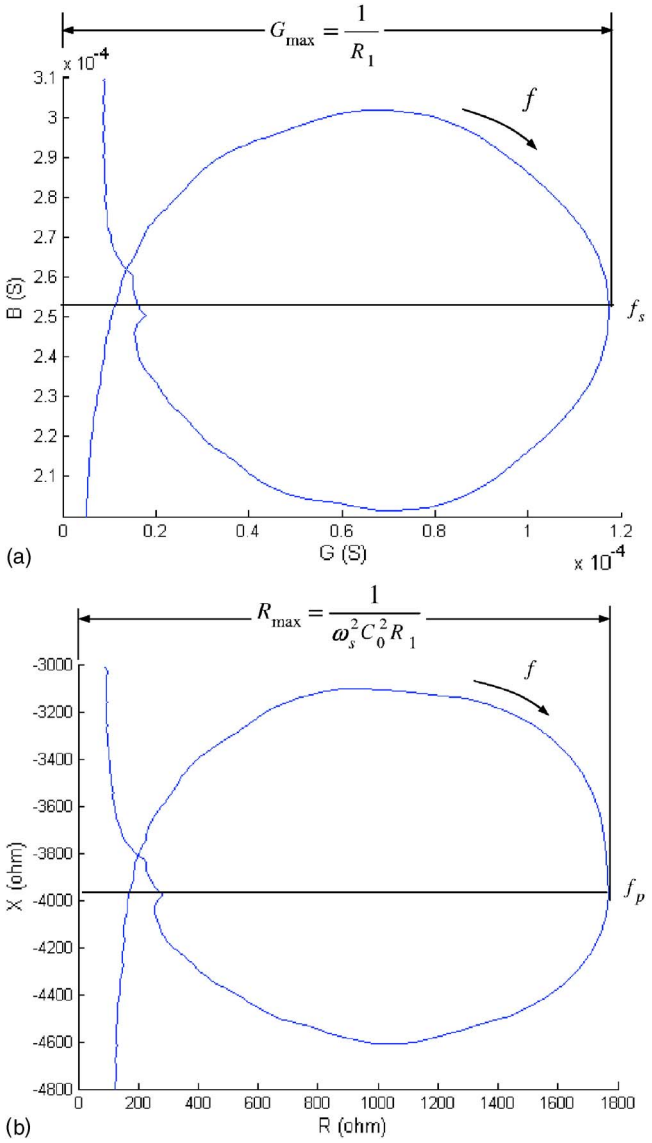

FIG. 6. (Color online) The measured Nyquist plots of the piezoelectric diaphragm without the added mass. (a) Electrical admittance $Y=G+jB$ and (b) electrical impedance $Z=R+jX$.

$$C_1 = C_f - C_0, \tag{3}$$

$$L_1 = \frac{1}{(2\pi f_s)^2 C_1}, \tag{4}$$

$$R_1 = \frac{1}{G_{\max}}, \tag{5}$$

$$Q = \frac{1}{2\pi f_s R_1 C_1}, \tag{6}$$

where C_f is the free capacitance of the PZT, which is measured as 7.167E-9 F at 1 kHz for the piezoelectric diaphragm.

2. The added-mass method

The resonance frequencies of the piezoelectric diaphragm without and with the added mass can be written as

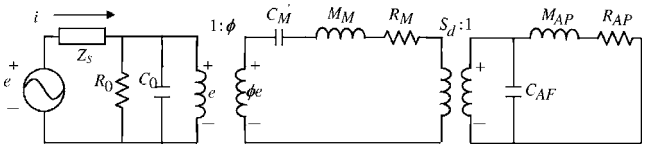

FIG. 7. The EMA analogous circuit of the piezoelectric buzzer.

$$\omega_n = \frac{1}{\sqrt{M_A C_A}}, \tag{7}$$

$$\omega_n = \frac{1}{\sqrt{(M_A + \Delta M_A) C_A}}, \tag{8}$$

where ΔM_A denotes the added mass expressed in the acoustical domain and M_A and C_A denote acoustical mass and compliance, respectively. Solving Eqs. (7) and (8) simultaneously for M_A and C_A yields

$$C_A = \frac{1}{\Delta M_A}\left(\frac{1}{\omega_n^2} - \frac{1}{\omega_n^2}\right), \tag{9}$$

$$M_A = \frac{1}{\omega_n^2 C_A}. \tag{10}$$

This corresponds to the mechanical mass and compliance,

$$M_M = M_A S_D^2, \tag{11}$$

$$C_M' = \frac{C_A}{S_D^2}, \tag{12}$$

where S_D is the effective area of the piezoelectric diaphragm (approximately 60% of the nominal area). The nonhomogeneity of the plate rather than the boundary condition leads to the large value of the effective area. Its central part is thicker than the peripheral, rendering the central part to vibrate almost as a rigid piston. Finally, the transduction factor (ϕ) and the mechanical resistance (R_M) can be estimated as follows:

$$\phi = \sqrt{\frac{C_1}{C_M}} = \sqrt{\frac{M_M}{L_1}}, \tag{13}$$

TABLE II. Lumped parameters of the piezoelectric buzzer.

Parameter	Value	Parameter	Value
f_p (Hz)	4931.3	$R_1(\Omega)$	3870.5
f_s (Hz)	4875.0	$R_0(\Omega)$	1.50E6
f_m (Hz)	4812.5	Q	40.6
f_n (HZ)	5018.8	M_M (kg)	5.25E−5
C_0 (F)	8.96E−9	C_M' (m/N)	2.08E−5
C_1 (F)	2.08E−10	R_M (N s/m)	3.86E−2
L_1 (H)	5.13	ϕ(N/V)	0.0032

$$R_M = \phi^2 R_1. \tag{14}$$

Following the preceding parameter identification procedure, lumped parameters of the piezoelectric diaphragm were calculated and summarized in Table II.

B. Frequency response simulation

After the lumped parameters of the piezoelectric diaphragm are identified, the response of the buzzer can be simulated on the basis of the EMA analogous circuit of Fig. 7. In the acoustical domain, the acoustical mass of port (M_{AP}), the acoustical resistance of port (R_{AP}), and the acoustical compliance of front cavity (C_{AF}) are calculated using the following formulas:[13]

$$M_{AP} = \frac{\rho_0}{\pi a_p^2}(t_c + 1.462 a_p), \tag{15}$$

$$R_{AP} = \frac{\rho_0}{\pi a_p^2}\sqrt{2\omega\mu}\left[\frac{t_c}{a_p} + 6.4\left(1 - \frac{\pi a_p^2}{b^2}\right)\right], \tag{16}$$

$$C_{AF} = \frac{V_{AF}}{\rho_0 c^2}, \tag{17}$$

where a_p is the radius of port, t_c is the thickness of front cavity, μ is the viscosity coefficient ($\mu = 1.56 \times 10^{-5}\mathrm{m}^2/\mathrm{s}$), b is the diameter of the piezoelectric diaphragm, V_{AF} is the volume of front cavity, c is the speed of sound ($c \approx 345$ m/s at the room temperature), and ρ_0 is the density of air ($\rho_0 = 1.21\ \mathrm{kg/m}^3$). It can be shown that the loop equations[15] corresponding to the analogous circuit of Fig. 7 are written as the following system of linear equations:

$$\begin{bmatrix} Z_S + Z_{EB} & -\phi Z_{EB} & 0 & 0 & 0 \\ Z_{EB} & -\phi Z_{EB} & -1 & 0 & 0 \\ 0 & Z_{ms} & -\phi & S_d & 0 \\ 0 & -S_d\left(M_{AP}s + \frac{1}{C_{AF}s}\right) & 1 & 0 & \frac{1}{C_{AF}s} \\ 0 & \frac{-S_d}{C_{AF}s} & 0 & 0 & M_{AP}s + \frac{1}{C_{AF}s} + R_{AP} \end{bmatrix} \begin{bmatrix} i \\ u \\ e \\ e' \\ i' \end{bmatrix} = \begin{bmatrix} V_g \\ 0 \\ 0 \\ 0 \\ 0 \end{bmatrix}, \tag{18}$$

where V_g is driving voltage, $s=j\omega$ is the Laplace variable, and

$$Z_{EB} = \frac{1}{C_0 S} \| R_0, \tag{19}$$

$$Z_{ms} = Z_M \approx M_M S + \frac{1}{C'_M S} + R_M. \tag{20}$$

Using the loop equations, the electrical impedance and the sound pressure output of the buzzer can be simulated.

C. Theory of dynamic vibration absorber

There is a common, but often overlooked, mistake in designing a resonant device of this kind. Since a piezoelectric buzzer is a narrow-band device, it is tempting to tune the resonant frequency of the acoustical system (ω_A) to coincide with that of the mechanical system (ω_M), i.e., $\omega_A=\omega_M$, such that the device would produce the maximum output when driven at this coincided frequency. Hence, instead of maximum response, the output turns out to be rather small at the driving frequency. In fact, counterintuitive phenomenon arises in the bass-reflex and bandpass designs of loudspeakers as well. Not much about its aspect has been reported in the previous research to date. It is worth exploring the physics underlying the coupled mechanical and acoustical resonators.

1. Dynamic vibration absorber

Consider a machine rotating with constant speed ω, as shown in Fig. 8(a). The displacement responses, $\bar{X}_1(\omega)$ and $\bar{X}_2(\omega)$, of this two degree-of-freedom system can be shown to be[11,12]

$$\bar{X}_1(\omega) = \frac{1}{\Delta(\omega)}(k_2 - \omega^2 m_2) F_{\text{eq}}, \tag{21}$$

$$\bar{X}_2(\omega) = \frac{1}{\Delta(\omega)} k_2 F_{\text{eq}}, \tag{22}$$

where ω is angular frequency, m_1 and k_1 are the mass and the spring constant of the rotating machine, m_2 and k_2 are the mass and the spring constant of the vibration absorber, F_{eq} is the unbalance force amplitude, and

$$\Delta(\omega) = (k_1 + k_2 - \omega^2 m_1)(k_2 - \omega^2 m_2) - k_2^2 = 0 \tag{23}$$

is the frequency-dependent characteristic equation. In general, the undamped dynamic vibration absorber is "tuned" for $k_1/m_1=k_2/m_2$ such that $\bar{X}_1(\omega)$ approaches zero at the frequency $\omega_0=\sqrt{k_1/m_1}=\sqrt{k_1/m_2}$, as shown in Fig. 8(b). This is the characteristic that is frequently exploited to suppress narrow-band vibrations of rotating machinery.

2. Design of resonant acoustical devices

The design of a resonant acoustical device, here a piezoelectric buzzer, shares quite similar electroacoustical structure with the preceding vibration absorber problem. Figure 9 shows this structure in the mechanical domain, where a serial

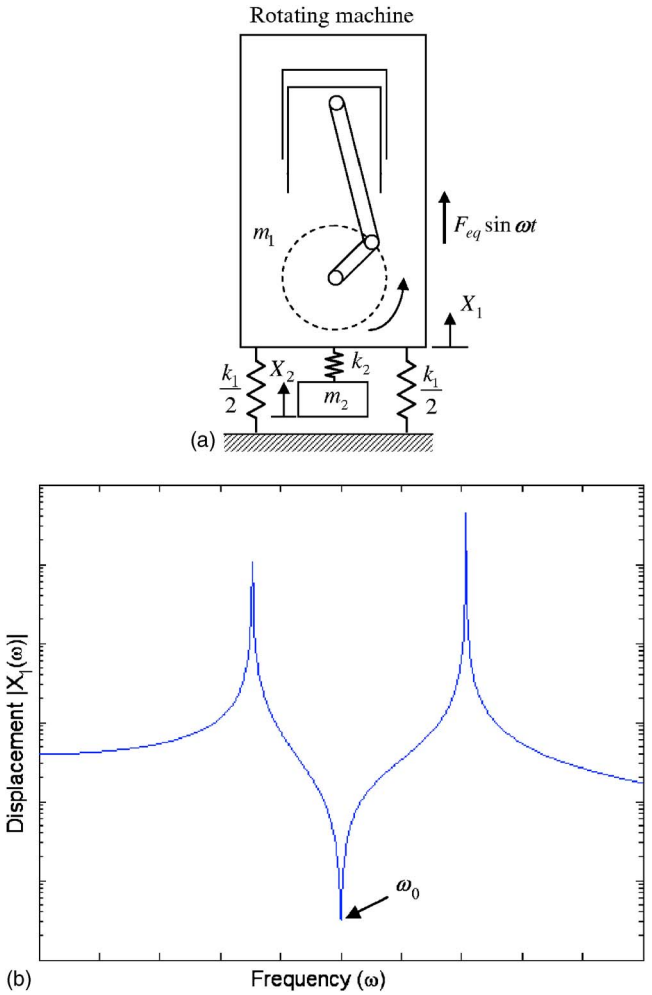

FIG. 8. (Color online) Dynamic vibration absorber. (a) A rotating machine attached with an absorber and (b) frequency response magnitude.

second-order oscillator circuit is coupled with a parallel second-order oscillator circuit. It is mathematically easier to derive the system characteristic equation by having a parallel resistance R_{AL} on the mechanical side, with R_{AP} neglected, in the circuit. Nevertheless, in deriving the design chart, only the undamped resonant frequencies are of concern. The actual position of the mechanical resistor is immaterial since both resistors are removed in the circuit of the coupled system. Note, however, that the port loss R_{AP} is considered in the constrained optimization procedures with the circuit of Fig. 3. When $\omega_A=\omega_M$, the motion of the mechanical system cancels that of the acoustical system, or alternatively viewed, the infinitely large impedance of the acoustical system

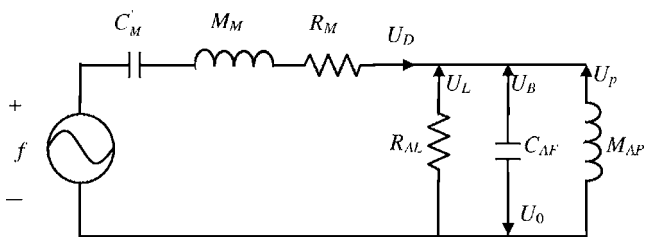

FIG. 9. A simplified analogous circuit of the piezoelectric buzzer expressed in the mechanical domain.

"blocks" the motion of the mechanical system. This is the feature that is frequently exploited to suppress vibrations, which forms the basis of vibration absorber theory. However, in the case of resonant acoustical devices, the naive approach of choosing equal resonant frequencies for both systems will result in an unexpected response null at $\omega_A = \omega_M$. This is obviously undesirable in the buzzer design. Contrary to vibration control, where one seeks to minimize the response, our purpose here in the acoustical design of buzzer is to maximize the sound pressure output, and it is the peaks of frequency response that we are after.

Let U_0 be the total velocity emitted from the diaphragm, the port, and the air leaks. From Fig. 9,

$$U_0 = U_D + U_P + U_L = -U_B, \tag{24}$$

where U_B is the net velocity entering the enclosure. The mechanical impedance and the acoustical impedance are given by

$$Z_M = M_M s + R_M + \frac{1}{C'_M s} = \frac{\frac{S^2}{\omega_M^2} + \frac{1}{Q_M}\frac{S}{\omega_M} + 1}{C'_M s}, \tag{25}$$

$$Y_A = C_{AF} s + \frac{1}{R_{AL}} + \frac{1}{M_{AP} s} = \frac{\frac{S^2}{\omega_A^2} + \frac{1}{Q_A}\frac{S}{\omega_A} + 1}{M_{AP} s}. \tag{26}$$

The total electrical impedance can be written as the sum of the mechanical impedance and the acoustical impedance:

$$Z_T = Z_M + \frac{1}{Y_A} = \frac{\Delta(s)}{C'_M s\left(\frac{S^2}{\omega_A^2} + \frac{1}{Q_A}\frac{S}{\omega_A} + 1\right)}, \tag{27}$$

where

$$\Delta(s) = \left(\frac{s^2}{\omega_M^2} + \frac{1}{Q_M^2}\frac{s}{\omega_M} + 1\right)\left(\frac{s^2}{\omega_A^2} + \frac{1}{Q_A}\frac{s}{\omega_A} + 1\right) + M_{AP} C'_M s^2 \tag{28}$$

denotes the characteristic equation, ω_M is the resonant frequency of the mechanical system (the piezoelectric diaphragm),

$$\omega_M = \sqrt{\frac{1}{M_M C'_M}}, \tag{29}$$

ω_A is the resonant frequency of the acoustical system (the cavity and port),

$$\omega_A = \sqrt{\frac{1}{M_{AP} C_{AF}}}, \tag{30}$$

and Q_M and Q_A are the quality factors of the mechanical system and the acoustical system, respectively, given by

$$Q_M = \frac{1}{R_m C'_M \omega_M}, \tag{31}$$

$$Q_A = \frac{R_{AL}}{C_{AF}\omega_A}. \tag{32}$$

It can be shown that the characteristic equation in Eq. (28) can be rewritten into an alternative form

$$\Delta = \frac{s^4}{\omega_0^4} + a_3\frac{s^3}{\omega_0^3} + a_2\frac{s^2}{\omega_0^2} + a_1\frac{s}{\omega_0} + 1 = 0, \tag{33}$$

where the frequency ω_0 and the coefficients a_1, a_2, and a_3 are defined as

$$\omega_0 = \sqrt{\omega_A \omega_M} = \frac{\omega_M}{\sqrt{\alpha}} = \omega_A\sqrt{\alpha}, \tag{34}$$

$$a_1 = \frac{1}{Q_M\sqrt{\alpha}} + \frac{\sqrt{\alpha}}{Q_A}, \tag{35}$$

$$a_2 = \frac{1}{\alpha} + \alpha + \frac{1}{Q_M Q_A} + \frac{\rho}{\alpha}, \tag{36}$$

$$a_3 = \frac{1}{Q_A\sqrt{\alpha}} + \frac{\sqrt{\alpha}}{Q_M}. \tag{37}$$

In these equations, the frequency ratio α and the mass ratio ρ are defined as

$$\alpha = \frac{\omega_M}{\omega_A} > 0, \tag{38}$$

$$\rho = \frac{M_{AP}}{M_M} > 0. \tag{39}$$

For undamped systems, where $Q_M \to \infty$ and $Q_A \to \infty$, the characteristic equation simplifies to

$$\Delta(S) = \alpha^2 r_M^4 - (1 + \alpha^2 + \rho) r_M^2 + 1 = 0 \tag{40}$$

in which the normalized frequency r_m is defined as

$$r_M = \frac{\omega}{\omega_M}. \tag{41}$$

Solving for the roots of the characteristic equation yields two undamped natural (resonance) frequencies. Note that the resonance frequencies of the coupled (mechanical and acoustical) system are generally different from, but strongly influenced by, those of the individual subsystems. According to Eq. (40), the resonance frequencies of the coupled system can be plotted versus the mass ratio ρ for various frequency ratios α. This gives the design charts shown in Fig. 10, in which the curves for mass ratio $\rho > 0$ are in used, while the curves for mass ratio $\rho \leqslant 0$ are only mathematical.

3. Acoustical design by the design chart

Assuming that the properties of the mechanical system are fixed, we now focus on the design of the acoustical

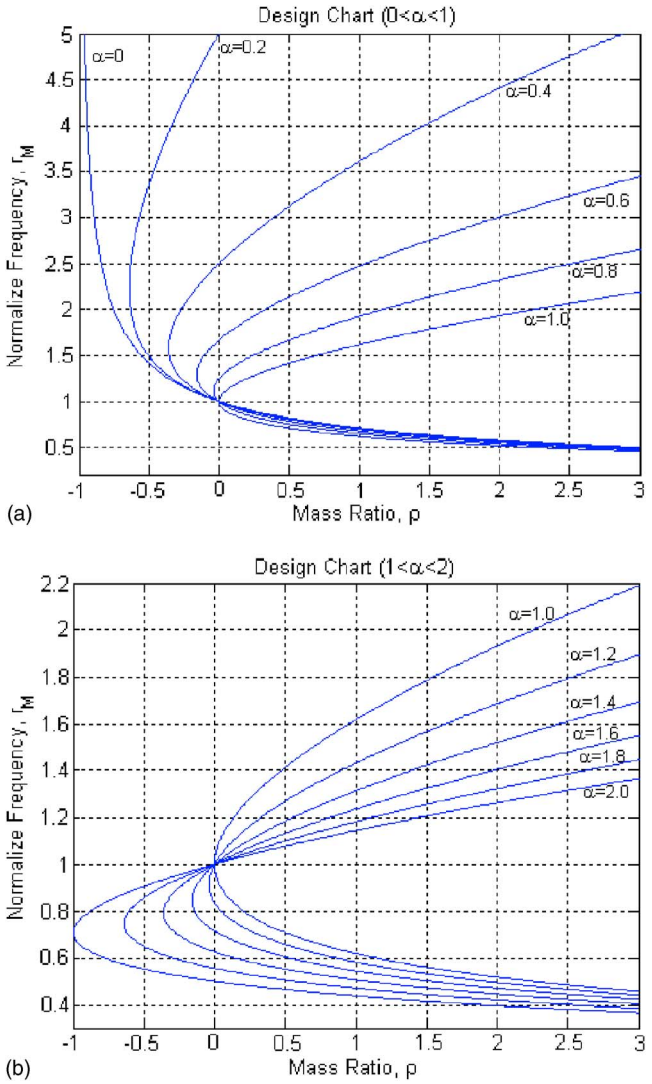

FIG. 10. (Color online) The design chart of the piezoelectric buzzer. (a) $0 \leqslant \alpha \leqslant 1$ and (b) $1 \leqslant \alpha \leqslant 2$.

system with the aid of the design chart. The design variables we wish to determine are the volume of cavity, the radius of port, and the length of duct. The design procedure is outlined as follows:

(1) Specify design constraints. Fix the mechanical resonant frequency ($f_M = \omega_M / 2\pi$) of the piezoelectric diaphragm. Assume $f_A = \omega_A / 2\pi < f_M$.
(2) Fix the first resonant frequency ($f_1 = \omega_1 / 2\pi$) of the coupled system (piezoelectric buzzer) at the driving frequency, e.g., 4 kHz.
(3) From the mechanical resonant frequency (f_M) and the first resonant frequency (f_1), calculate the normalized frequency ($r_1 = f_1 / f_M$).
(4) Choose a mass ratio (ρ) and determine the acoustical mass (M_{AP}).
(5) Assume a value for the radius of port (a_p). Determine the length of duct (t_c) according to Eq. (15).
(6) Choose the design curve (α) that corresponds to the normalize frequency and mass ratio determined previously.
(7) Determine the acoustical resonant frequency, $f_A = f_M / \alpha$.
(8) Per Eq. (30), calculate the acoustical compliance (C_A) based on M_{AP} and f_M. Also calculate the cavity volume according to Eq. (17).

III. OPTIMAL DESIGN OF THE PIEZOELECTRIC BUZZER

The optimization design procedure is based on the preceding piezoelectric buzzer model. The purpose here is to find the best mechanical and acoustical parameters of the piezoelectric buzzer to attain the maximum sound pressure output at the driving frequency under prescribed constraints. The design chart method and the Sequential Quadratic Programming (SQP) algorithm are employed to find the optimal parameters.

A. Sequential quadratic optimization theory and syntax

A brief review of a nonlinear programming technique, the SQP algorithm, is given in this section.[16–18] In the solution process of the SQP method, a nonlinear programming problem is first converted to a sequence of unconstrained minimization problems. A Quadratic Programming (QP) subproblem is then solved at each iteration. Consider the following nonlinear programming problem:[16]

$$\text{Minimize } f(\mathbf{x})$$

$$\text{subject to} \begin{cases} h_i(\mathbf{x}) = 0, & i = 1, \ldots, p \\ h_j(\mathbf{x}) \leqslant 0, & j = 1, \ldots, m, \end{cases} \tag{42}$$

where $\mathbf{x} \in R^n$ is the design variable vector, $f: R^n \to R$, being the cost function, $h_i: R^p \to R$, being the equality constraints, and $h_j: R^m \to R$, being the inequality constraints. Other types of linear constraints including matrix and bound types can all be cast into the generic form in Eq. (42). The SQP method requires a quadratic model for the objective function and a linear model for the constraint. This is done by formulating the QP subproblem based on a quadratic approximation to the Lagrangian function,[16]

$$L(\mathbf{x}, \boldsymbol{\mu}, \mathbf{v}) = f(\mathbf{x}) + \sum_{i=1}^{p} \boldsymbol{\mu}_i h_i(\mathbf{x}) + \sum_{i=1}^{m} \mathbf{v}_j [h_j(\mathbf{x}) + \mathbf{g}_j^2], \tag{43}$$

where $\boldsymbol{\mu}_i$ and $\mathbf{v}_j$ are the Lagrange multipliers, and $\mathbf{g}_j$ are termed the slack variables. By the Kuhn-Tucker conditions,[16] it suffices to solve the unconstrained optimization problem using the above-mentioned Lagrangian function. In practice, however, a simplified problem can be obtained by approximating the constraints (up to the first order) and the cost function (up to the second order) using the Taylor expansion. Thus, at the kth iteration, the SQP algorithm generates a search direction, $\mathbf{d}_k$, for the following QP subproblem:

$$\text{Minimize } \nabla f_k^T(\mathbf{x})\mathbf{d}_k + \tfrac{1}{2}\mathbf{d}_k^T\mathbf{B}_k\mathbf{d}_k$$

$$\text{subject to} \begin{cases} h_i(\mathbf{x}_k) + \nabla h_i^T(\mathbf{x}_k)\mathbf{d}_k = 0, & i = 1, \ldots, l \\ h_j(\mathbf{x}_k) + \nabla h_j^T(\mathbf{x}_k)\mathbf{d}_k \leqslant 0, & j = l+1, \ldots, m. \end{cases} \tag{44}$$

In Eq. (44), ∇f, ∇h_i, and ∇h_j denote the gradients of the cost function, the ith equality constraint, and the jth inequality constraint, respectively, $\mathbf{d}_k$ is the direction of search in the design space. The matrix $\mathbf{B}_k$ is a positive definite approximation to the Hessian matrix of the Lagrangian function $L(\mathbf{x}_k, \boldsymbol{\mu}_k, \mathbf{v}_k)$.[16–18] $\mathbf{B}_k$ is updated by using the Broyden, Fletcher, Goldfarb, and Shanon method,

$$\mathbf{B}_{k+1} = \mathbf{B}_k + \frac{\hat{\mathbf{y}}^T\hat{\mathbf{y}}}{\mathbf{s}^T\hat{\mathbf{y}}} - \frac{\mathbf{B}_k\mathbf{s}\mathbf{s}^T\mathbf{B}_k}{\mathbf{s}^T\mathbf{B}_k\mathbf{s}}, \tag{45}$$

where

$$\mathbf{s} = \mathbf{x}_{k+1} - \mathbf{x}_k, \tag{46}$$

$$\hat{\mathbf{y}} = t[\nabla_x L(\mathbf{x}_{k+1}, \boldsymbol{\mu}_{k+1}, \mathbf{v}_{k+1}) - \nabla_x L(\mathbf{x}_k, \boldsymbol{\mu}_k, \mathbf{v}_k)] + (1-t)\mathbf{B}_k\mathbf{s}. \tag{47}$$

Here, $\hat{\mathbf{y}}$ is obtained using the damping factor t in order to guarantee that $\mathbf{B}_{k+1}$ is sufficiently positive definite at the solution point. A positive definite Hessian is maintained, provided $\hat{\mathbf{y}}^T\hat{\mathbf{y}}/\mathbf{s}^T\hat{\mathbf{y}}$ is positive at each update and that $\mathbf{B}_k$ is initialized with a positive definite matrix. There are many numerical methods to solve a QP problem, e.g., the modified simplex method or the Kuhn-Tucker procedures.[17] The solution of $\mathbf{d}_k$ is used to update the estimate of $\mathbf{x}$,

$$\mathbf{x}_{k+1} = \mathbf{x}_k + \alpha_k\mathbf{d}_k. \tag{48}$$

In the update equation, the step size parameter α_k is determined by an appropriate line search procedure so that a sufficient decrease in a merit function such as the Lagrangian function is obtained.

The preceding optimization formalism was employed to solve the piezoelectric buzzer design problem on the platform of MATLAB.[20] The syntax of the constrained optimization takes the following form augmented with various linear equality and inequality constraints:

$$\min_x f(\mathbf{x}) \text{ subject to } \begin{aligned} &\mathbf{c}(\mathbf{x} \leqslant 0), \\ &\mathbf{c}_{\text{eq}}(\mathbf{x}) = 0, \\ &\mathbf{A}\mathbf{x} \leqslant \mathbf{b}, \\ &\mathbf{A}_{\text{eq}}\mathbf{x} = \mathbf{b}_{\text{eq}}, \\ &\mathbf{I}\mathbf{b} \leqslant \mathbf{x} \leqslant \mathbf{u}\mathbf{b}, \end{aligned} \tag{49}$$

where $\mathbf{x}$ is the design variable vector, $\mathbf{b}$, $\mathbf{b}_{\text{eq}}$, $\mathbf{lb}$, and $\mathbf{ub}$ are constant vectors, $\mathbf{A}$ and $\mathbf{A}_{\text{eq}}$ are constraint matrices, $\mathbf{c}(\mathbf{x})$ and $\mathbf{c}_{\text{eq}}(\mathbf{x})$ are constraint functions that return vectors, and $f(\mathbf{x})$ is the cost function that returns a scalar. $f(\mathbf{x})$, $\mathbf{c}(\mathbf{x})$, and $\mathbf{c}_{\text{eq}}(\mathbf{x})$ can be nonlinear functions. In the piezoelectric buzzer design problem considered herein, the on-axis sound pressure at the driving frequency 4 kHz of piezoelectric buzzer is defined as the cost function.

B. Constrained optimization method

In the following, two kinds of optimal design problems of piezoelectric buzzer shall be examined. The first problem focuses on the design of the acoustical system alone because of the closer acoustical resonance to the driving frequency. In this case, the volume of cavity, the port size, and the duct length are to be determined, and the parameters of the mechanical system are assumed to be fixed. The second problem focuses on the design of both mechanical and acoustical systems, where, in addition to the parameters of the first problem, the parameters of the piezoelectric diaphragm are to be determined.

1. Optimal design of the acoustical system alone

In this case, constraints are placed on design factors including acoustical mass (M_{AP}), acoustical compliance (C_{AF}), acoustical resistance (R_{AP}), the first resonant frequency of piezoelectric buzzer (f_1=4 kHz), characteristic equation of piezoelectric buzzer [$\Delta(s)$=0], radius of port (a_p) and height of front cavity (d_{AF}). Among these, a_p and t_c are selected to be the design variables for optimization. In terms of the forgoing optimal formalism,

$$\max \text{SPL}(a_p, t_c)$$

$$\text{st.} \begin{cases} 0.001 \leqslant a_p \leqslant 0.002 \\ 0.00308 \leqslant d_{AF} \leqslant 0.005 \\ 1\text{E}-7 \leqslant M_{AP} \leqslant 1\text{E}-5 \\ 2\text{E}5 \leqslant R_{AP} \leqslant 2\text{E}7 \\ 1\text{E}-4 \leqslant C_{AF} \leqslant 3\text{E}-4 \\ f_1 = 4000 \\ \Delta = 0 \end{cases} \tag{50}$$

2. Optimal design of both mechanical and the acoustical systems

The second case aims at the optimal design of the cavity and piezoelectric diaphragm. Constraints are placed on design factors including acoustical mass (M_{AP}), acoustical compliance (C_{AF}), acoustical resistance (R_{AP}), the first resonant frequency of piezoelectric buzzer (f_1=4 kHz), mechanical quality factor (Q_M), characteristic equation of piezoelectric buzzer [$\Delta(s)$=0], transduction factor (ϕ), mechanical mass (M_M), mechanical compliance (C'_M), mechanical resistance (R_M), radius of port (a_p), height of the front cavity (d_{AF}), free capacitance of piezoelectric diaphragm (C_f), and the clamped capacitance of piezoelectric diaphragm (C_0). From these parameters, M_M, C'_M, R_M, a_p, d_{AF}, C_f, and C_0 are selected to be the design variables for optimization. In terms of the forgoing optimal formalism,

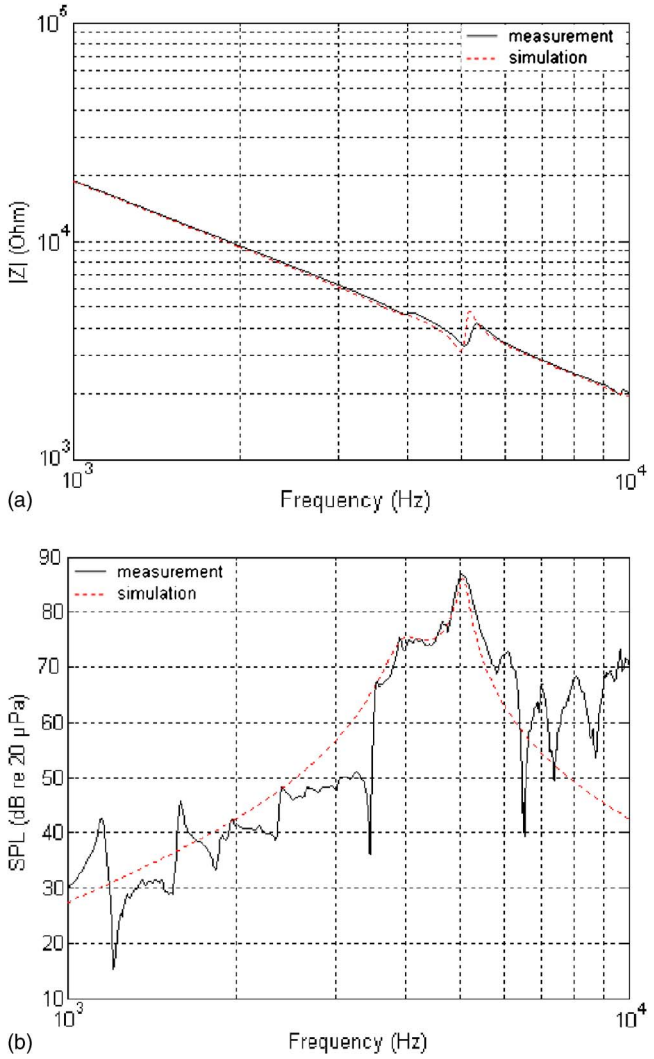

FIG. 11. (Color online) Frequency responses of piezoelectric buzzer obtained from the experiment and simulation. (a) Electrical impedance and (b) on-axis SPL.

$$\max \ \mathrm{SPL}(a_p, d_{AF}, M_M, C_M, R_M, C_f, C_0)$$

$$\text{st}\begin{cases} 0.001 \leqslant a_p \leqslant 0.002 \\ 0.0015 \leqslant d_{AF} \leqslant 0.005 \\ 4\mathrm{E}-5 \leqslant M_M \leqslant 7\mathrm{E}-5 \\ 1\mathrm{E}-5 \leqslant C_M \leqslant 5.5\mathrm{E}-5 \\ 0.01 \leqslant R_M \leqslant 0.08 \\ 8\mathrm{E}-9 \leqslant C_f \leqslant 11\mathrm{E}-9 \\ 7\mathrm{E}-9 \leqslant C_0 \leqslant 10\mathrm{E}-9 \\ 0.003 \leqslant \phi \leqslant 0.006 \\ 1\mathrm{E}-7 \leqslant M_A \leqslant 1\mathrm{E}-5 \\ 2\mathrm{E}5 \leqslant R_A \leqslant 2\mathrm{E}-7 \\ 1\mathrm{E}-4 \leqslant C_A \leqslant 9\mathrm{E}-4 \\ 30 \leqslant Q_M \leqslant 50 \\ f_1 = 4000 \\ \Delta = 0 \\ C_1 L_1 = C_M' M_M \end{cases} \tag{51}$$

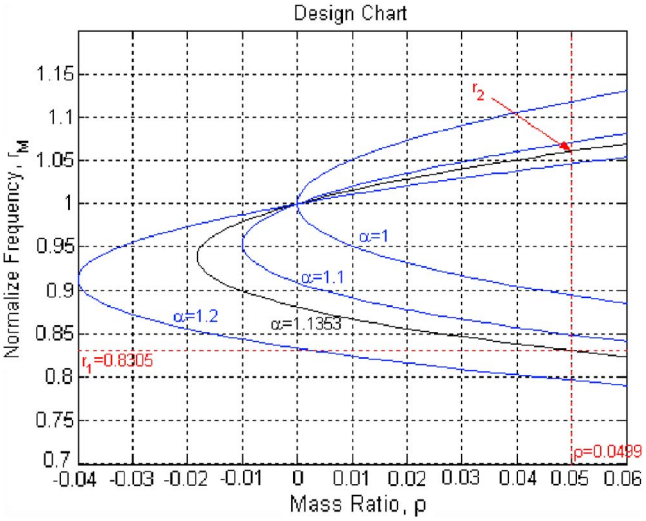

FIG. 12. (Color online) Close-up view of the design chart for the present buzzer design.

IV. NUMERICAL AND EXPERIMENTAL INVESTIGATIONS

Simulation and experimental investigations are undertaken in this paper to validate the aforementioned design optimization techniques of the piezoelectric buzzer. A 1.5 V_{rms} swept sine signal is generated to drive the piezoelectric buzzer, with the frequency ranging from 10 Hz to 20 kHz. On-axis sound pressure response was measured by a microphone positioned at 10 cm away from the piezoelectric buzzer.

A. Response simulation and experimental investigation

A simulation of the buzzer response was carried out on the basis of the lumped parameter model identified previously. Figures 11(a) and 11(b) are the electrical impedance and the on-axis SPL obtained from the simulation and experiment, respectively. The simulated electrical impedance (dashed line) is in reasonable agreement with that of the measured results (solid line). The on-axis sound pressure responses of the simulation and measurement are also in good agreement within the working range, 3.5–5.5 kHz. Except for some minor discrepancies due to unmodeled structural and acoustical modes, the main features, such as the main peaks, are well captured by the lumped parameter model.

B. Optimal design by the design chart

Suppose only acoustical design is of interest and mechanical parameters are fixed, the optimal design of the cavity and duct of the buzzer can be readily obtained from the design chart. Assume that the piezoelectric diaphragm resonant frequency is greater than the acoustical resonant frequency ($f_M > f_A$). The objective is to "lock" the first peak of the SPL of the coupled buzzer system onto the driving frequency 4 kHz. The design variables are selected to be the port radius and the duct length. According to the design chart shown in Fig. 12 and the procedure detailed in the preceding section, the optimal parameters including the port radius

TABLE III. Results obtained using the design chart method.

Parameters	Original	Optimal	Difference
t_c (mm)	0.76	2.28	–200.0%
a_p (mm)	1.065	1.5	40.8%
M_{AP} (kg/m^4)	786.81	766.01	–2.6%
R_{AP} (N s/m^5)	3.31E6	2.14E6	–35.3%
ρ	0.0513	0.0499	–2.7%
f_a(Hz)	4157.4	4242.20	2.0%
α	1.157	1.135	–1.9%
SPL (dB) at 4 kHz	73.3	79.9	6.6 dB

(a_p), the duct length (t_c), and the acoustical resistance (R_{AP}) are found and summarized in Table III. In this case, the normalized frequencies r_1=0.8305 and the mass ratio ρ =0.0499, the frequency ratio α=1.1353.

Yet another approach by incorporating a duct in the design is also a viable option that does not require an unduly increase of cavity volume. The cross section of this design is shown in Fig. 13(a). The photo of a mockup of the optimal obtained using the preceding design chart method is shown in Fig. 13(b). The results obtained using the method of design chart shown in Table III reveal that the duct length is increased by 200% to 2.28 mm, and the duct radius is increased by 40.8% to 1.5 mm. The increase of duct length and radius results in the decrease of M_{AP} and R_{AP}. Alternatively, one may opt to increase the cavity volume and the duct radius to reduce C_{AF} and R_{AP}. However, this approach by increasing the cavity volume is generally unacceptable in practical design of buzzers. As can be seen in the optimal results, a 6.6 dB increase of on-axis SPL is achieved at 4 kHz with the increased radius and length of the duct. The simulated (dashed line) and the measured (solid line) electrical impedances and SPL frequency responses of the design are verified in Figs. 14(a) and 14(b). In Fig. 14(a), the simulation and the measurement results of electrical impedance are in good agreement at the first and the second resonance frequencies. In Fig. 14(b), the on-axis sound pressure responses of the simulation and measurement are also in good agreement between the first and the second resonance peaks. Thus, the improvement of the measured SPL over nonoptimal design is approximately 6.6 dB.

The guidelines of using the design chart can be summarized as follows. Reducing the acoustical mass (M_{AP}) and acoustical resistance (R_{AP}) will increase the SPL at the peak. However, reducing M_{AP}, equivalently, the mass ratio (ρ) will shift the acoustical resonant frequency (f_A) to a higher frequency. In case of a buzzer design, the preferred strategy is to select a lower mass ratio and a design curve with smaller frequency ratio (α) in the design chart. After these search steps, a satisfactory design can generally be found.

C. Optimal design by the constrained optimization procedure

In this section, the aforementioned optimization technique is applied to two cases. First, only the acoustical parameters are to be optimized. Second, both the mechanical and the acoustical parameters are to be optimized. The SQP constrained optimization algorithms are applied to search for optimal parameters of the coupled diaphragm-cavity system. Table IV summarizes the search results for the first case, where the duct radius is increased by 45.3% to 1.547 mm and the height of front cavity is increased by 62.3% to 5.0 mm. The on-axis SPL improvement at 4 kHz achievable by the optimal design is 5.8 dB. It should be noted that an increase of duct radius will lead to reduction of the acoustical mass and, hence, the acoustical resonant frequency. In addition, increase of the height of the front cavity will lead to the increase of the cavity volume and, hence, the acoustical compliance.

Table V summarizes the search results of the cavity-diaphragm parameters for the second case. For the acoustical

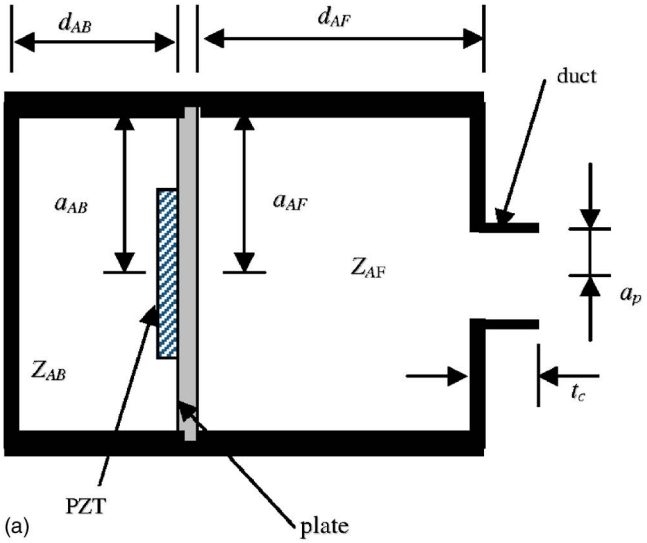

FIG. 13. (Color online) The piezoelectric buzzer with a duct resulting from the design chart method. (a) Cross-sectional diagram and (b) photo of the mockup.

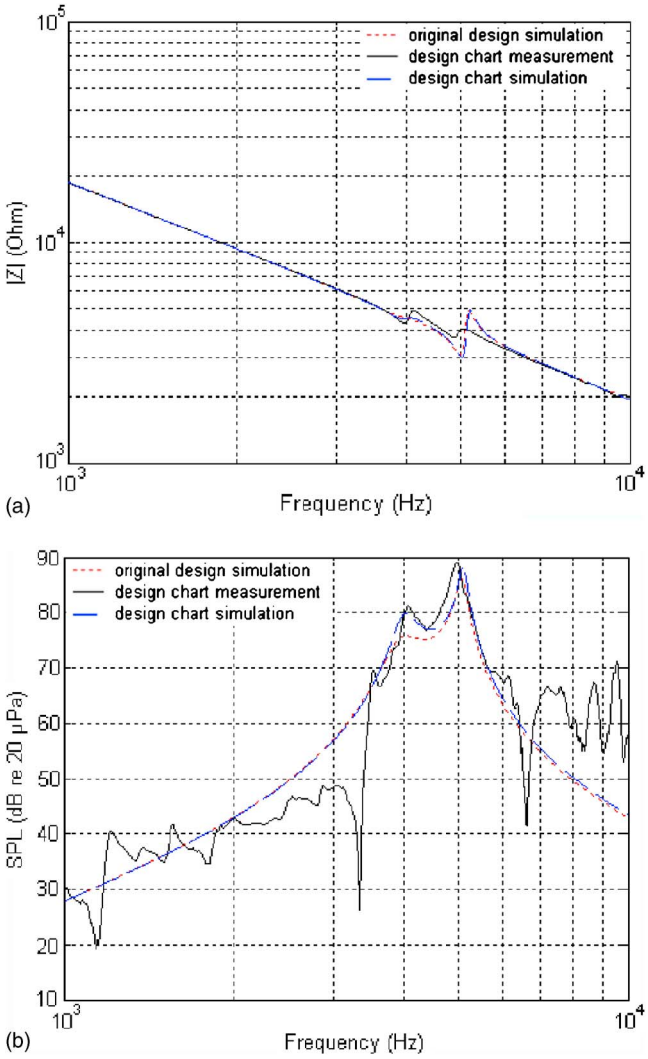

FIG. 14. (Color online) Comparison of the original design and the optimal design using the design chart method. (a) Electrical impedance and (b) on-axis SPL.

parameters, the duct radius is increased by 3.3% to 1.1 mm and the height of the front cavity is reduced by −38.3% to 1.9 mm. For the mechanical parameters, the mechanical mass is increased by 19.4% to 6.27E−2 g, whereas the mechanical compliance is increased by 10.1% to 2.29E −5 m/N. However, the electrical parameters remain almost unchanged. In addition, the resonant frequency of the structural system (f_M=4201 Hz) is lower than the resonant frequency of the acoustical system (f_A=5283 Hz). The resonant frequency of the structural system is close to the driving frequency at 4 kHz. The on-axis SPL improvement at 4 kHz achievable by this optimal design is 9.6 dB.

TABLE IV. Results obtained using the first optimal design that optimizes the acoustical system alone.

Parameters	Original	Optimal	Difference
a_p (mm)	1.065	1.547	45.3%
d_{AB} (mm)	3.08	5.0	62.3%
C_{AF} (m^5/N)	1.86E-12	3.02E-12	62.4%
M_{AP} (kg/m^4)	786.81	486.48	−38.2%
R_{AP} (N s/m^5)	3.31E6	1.48E6	−55.2%
ρ	0.0513	0.0317	−38.2%
f_a(Hz)	4157.4	4149.72	−0.2%
α	1.157	1.160	0.3%
SPL(dB) at 4 kHz	73.3	79.1	5.8 dB

TABLE V. Results obtained using the second optimal design that optimizes both mechanical and acoustical systems.

Parameters	Original	Optimal	Difference
a_p (mm)	1.065	1.1	3.3%
d_{AB} (mm)	3.08	1.9	−38.3%
M_M (kg)	5.25E-5	6.27E-5	19.4%
C'_M (m/N)	2.08E-5	2.29E-5	10.1%
R_M (N s/m)	0.0386	0.0386	0.0%
C_f (F)	9.17E-9	9.17E-9	0.0%
C_0 (F)	8.96E-9	8.96E-9	0.0%
C_{AF} (m^5/N)	1.86E-12	1.16E-12	−37.6%
M_{AP} (kg/m^4)	786.81	786.81	0.0%
R_{AP} (N s/m^5)	3.31E6	3.31E6	0.0%
ρ	0.0513	0.0482	−6.0%
f_m (Hz)	4812.4	4201	−12.7%
f_a (Hz)	4157.4	5283	27.1%
α	1.157	0.795	−31.3%
Q_M	40.6	42.9	5.7%
C_1 (F)	2.08E-10	1.82E-010	−12.5%
L_1 (H)	5.13	7.80	52.0%
R_1 (Ω)	3870.5	4874.1	25.9%
ϕ	0.0032	0.0028	−12.5%
SPL(dB) at 4 kHz	73.3	82.9	9.6 dB

For this optimal design, the electrical impedance and the SPL responses are simulated and shown in Figs. 15(a) and 15(b), respectively. The dashed line represents the original nonoptimal design. The dotted line represents the design using the first acoustical optimization approach. The solid line represents the design using the second mechanical and acoustical optimization approach. From Fig. 15(a), the electrical impedances of the original design and the first acoustic optimal designs are in reasonable agreement. However, the overall level of impedance of the original design and first optimal design are higher than the second optimal design. The response of the original design and first optimal design peak at 5 kHz (the second resonance), whereas the response of the second optimal design peaks at 4 kHz. In 15(b), the on-axis SPL responses of the second design is greater than the first design at the driving frequency 4 kHz, and both are greater than the SPL of the original nonoptimal design at 4 kHz. Specifically, the SPLs at the driving frequency 4 kHz of the first optimal design and the second optimal design are increased by approximately 5.8 and 9.6 dB, respectively, over the original nonoptimal design. The SPL response at 4 kHz of the second optimal design (82.9 dB) is higher than the first optimal design (79.1 dB) by 3.8 dB. Note that the structural resonant frequency of the second optimal design is near the driving frequency, while in the first optimal design the acoustical resonant frequency is near the driving frequency. Summarizing, a higher level of acoustic pressure appears for the resonant frequency near the original structural resonant frequency. This fact can be utilized for further im-

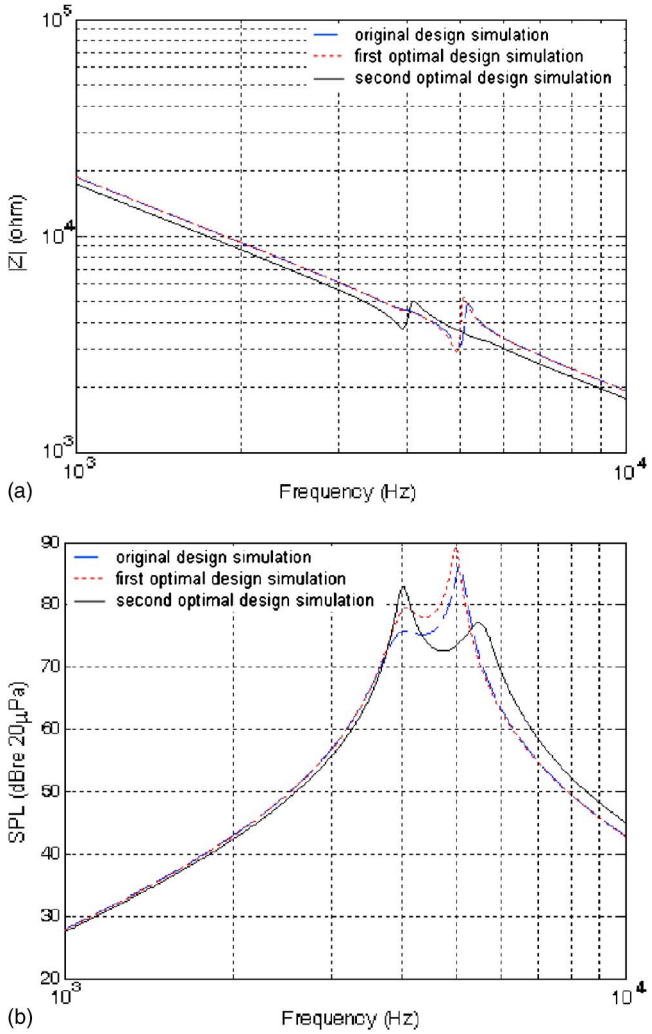

FIG. 15. (Color online) Comparison of the original design and the optimal designs using two constrained optimization approaches. (a) Electrical impedance and (b) on-axis SPL.

provement of the construction of the buzzer. The optimal result shows that the SPL attainable at the driving frequency can be significantly increased over the nonoptimal design. In addition, the resonant frequency of the structural system should be near the driving frequency of the piezoelectric buzzer. This design strategy proves effective in achieving a much improved performance, with the first resonant frequency fixed at 4 kHz.

V. CONCLUSIONS

An optimization technique has been presented in the paper for designing piezoelectric buzzers. An insightful inspection revealed that this buzzer problem can be closely related to the dynamic vibration absorber theory. A design chart was devised to design piezoelectric buzzers by exploiting the same mechanism, but opposite strategy, as the vibration absorber design. The guidelines of using the design chart were summarized in the paper. In order to establish a simulation platform for design optimization, a special kind of experimental identification procedure was also developed to estimate the lumped parameters required in the EMA analogous circuit. Using the simulation platform, electrical impedance and on-axis sound pressure response can be predicted by solving loop equations of the analogous circuit. The resonance frequencies of the coupled system are generally different from those of the individual subsystems. From the characteristic equation, the resonance frequencies of the coupled mechanical and acoustical system can be calculated. Maximum acoustical output can thus be attained by locking the resonance peak to the driving frequency.

Apart from the design chart method, constrained optimization techniques were also employed to find the design that maximizes the sound pressure output of the buzzer under practical constraints. Two approaches were applied in the optimization: acoustical-system-alone approach and mechanical-acoustical system approach. Both designs obtained using the optimization procedures provide significant performance improvement over the original design in terms of sound pressure output. However, the benefit of optimizing both mechanical and acoustical parameters is preferred over optimizing the acoustical parameters alone.

ACKNOWLEDGMENTS

The work was supported by China Steel Corporation and the National Science Council in Taiwan, Republic of China, under Project No. NSC 93-2212-E009-008.

[1]G. Caliano, N. Lamberti, A. Iula, and M. Pappalardo, "A piezoelectric bimorph static pressure sensor," Sens. Actuators, A, **46**, 176–178 (1995).
[2]C. I. Tseng and W. J. Liou, "Simulation of a bimorph transducer under acoustic excitation," Comput. Struct., **59**, 141–148 (1996).
[3]A. B. Dobrucki and P. Pruchnicki, "Theory of piezoelectric axisymmetric bimorph," Sens. Actuators, A, **58**, 203–212 (1997).
[4]Q. Wang, S. T, Quek, C. T. Sun, and X. Liu, "Analysis of piezoelectric coupled circular plate," Smart Mater. Struct., **10**, 229–239 (2001).
[5]B. Aronov, "The energy method for analyzing the piezoelectric electroacoustic transducers," J. Acoust. Soc. Am., **117**, 210–220 (2005).
[6]B. Aronov, "The energy method for analyzing the piezoelectric electroacoustic transducers. II (With the examples of the flexural plate transducer)," J. Acoust. Soc. Am. **118**, 627–637 (2005).
[7]M. R. Bai and Y. Lu, "Optimal implementation of miniature piezoelectric panel speakers using the Taguchi method and Genetic algorithm," J. Vibr. Acoust., **126**, 359–369 (2004).
[8]F. L. Wen, S. C. Mou, and M. Ouyang, "Design and construction of shaft-driving type piezoceramic ultrasonic motor," Ultrasonics **43**, 35–47 (2004).
[9]A. Caronti, G. Caliano, and M. Pappalardo, "An accurate model for capacitive micromachined ultrasonic transducers," IEEE Trans. Comput.-Aided Des., **49**, 159–168 (2002).
[10]Q. Gallas, R. Holman, T. Nishida, B. Carroll, M. Sheplak, and L. Cattafesta, "Lumped element modeling of piezoelectric-driven synthetic jet actuators." AIAA J., **41**, 240–247 (2003).
[11]F. S. Tse, I. E. Morse, and R. T. Hinke, *Mechanical Vibrations: Theory and Applications* (Allyn & Bacon, Boston, MA, 1978).
[12]L. Meirovitch, *Element of Vibration Analysis* (McGraw-Hill, New York, 1986).
[13]W. M. Leach, Jr., *Introduction to Electroacoustics and Audio Amplifier Design* (Kendall-Hunt, Dubuque, IA, 2003).
[14]L. L. Beranek, *Acoustics* (Acoustical Society of America, Melville, NY 1996).
[15]C. A. Desoer and E. S. Kuh, *Basic Circuit Theory* (McGraw-Hill, New York, 1969).
[16]P. E. Gill, W. Murry, and M. H. Wright, *Practical Optimization* (Academic, New York, 1981).
[17]J. S. Arora, *Introduction to Optimum Design* (McGraw-Hill, New York 1989).
[18]M. A. Bhatti, *Practical Optimization Methods with Mathematica Applications* (Springer, Berlin, 2000).
[19]IEEE, *IEEE Standard on Piezoelectricity* (New York, 1987).
[20]Math Works, "Matlab optimization toolbox" (http://www.mathworks.com/products/optimization/). Last viewed 7/23/2007.